Measurements of ^{89}Y(n,2n)^{88}Y and ^{89}Y(n,3n)^{87}Y, ^{87m}Y cross sections for fast neutrons at KIRAMS

Eun Jin In[1], Sang-In Bak[1], Cheolmin Ham[1], Do Yoon Kim[1], Hyunjeong Myung[2], Chungbo Shim[2], Jae Won Shin[3], Kyung Joo Min[1], Yujie Zhou[1], Tae-Sun Park[2], Seung-Woo Hong[2,a], and V.N. Bhoraskar[4]

[1] Department of Energy Science, Sungkyunkwan University, Suwon 16419, Korea
[2] Department of Physics, Sungkyunkwan University, Suwon 16419, Korea
[3] Department of Physics, Soongsil University, Seoul 06978, Korea
[4] Department of Physics, S.P. Pune University, Pune 411007, India

Abstract. A proton cyclotron MC-50 in Korea Institute of Radiological & Medical Science (KIRAMS) is used to carry out neutron activation experiments with Y_2O_3 targets irradiated with neutron beams of a continuous spectrum produced by proton beams on a thick beryllium target. Neutrons are generated by ^{9}Be (p, n) reaction with an incident proton intensity of 20 μA. The neutron spectra generated by proton beams of 30, 35, and 40 MeV are calculated by GEANT4 simulations. Nb powders are used for neutron flux monitoring by measuring the activities of ^{92m}Nb through the reaction ^{93}Nb (n, 2n). By using a subtraction method, the average cross section of ^{89}Y(n,2n) and ^{89}Y(n,3n) reactions at the neutron energies of 29.8 $\pm$ 1.8 MeV and 34.8 $\pm$ 1.8 MeV are extracted and are found to be close to the existing cross sections from the EXFOR data and the evaluated nuclear data libraries such as TENDL-2015 or EAF-2010.

1. Introduction

In the development of fast neutron systems, such as an Accelerator Driven System [1], nuclear data for neutron induced reactions at energies above 20 MeV are required, but they are not well known. For example, it is known that the content of Yttrium can improve the corrosion resistance of Zirconium-base alloy, but the data on ^{89}Y (n, 2n) cross sections were mostly reported up to the neutron energy of 30 MeV [2,3], and only a few data exist above 30 MeV [4]. Also, the data on ^{89}Y (n, 3n) reactions at neutron energies above 30 MeV are only scarcely measured with large uncertainties [5]. In this work, we thus consider the neutron induced reactions of Yttrium for fast neutrons.

However, in the high energy region above 20 MeV, the measurement of cross sections poses difficulties in the measurement and analysis because mono-energetic neutron beam is not easy to get. To obtain an accurate (n, xn) cross section, a mono-energetic neutron facility is needed. Neutron time-of-flight (n-TOF) facilities are developed and available worldwide [6,7]. Quasi-mono-energetic neutrons produced by ^{7}Li(p,n) and ^{9}Be(p,n) reactions are also used for the measurement of cross sections of neutron induced reactions in the high energy region [8,9]. In the present work, however, we used neutron beams with continuous energy spectra and attempted to extract ^{89}Y (n, 2n) and ^{89}Y (n, 3n) cross sections. Neutrons are produced by using the MC-50 cyclotron of the Korea Institute of Radiological and Medical Sciences (KIRAMS) through the ^{9}Be (p, n) reactions. From a broad continuous neutron beam generated by a proton beams impinging a thick Be target, we extracted (n, xn) cross sections by using a subtraction method.

2. Neutron spectra

Neutrons were produced by proton beams of 30, 35, and 40 MeV on a Be target of thickness of 10.5 mm, and the neutron spectra were obtained by using the GEANT4 code [10] with a data-based hadronic model discussed in Ref. [11]. Since the Be target is thick, the resulting neutron spectra were continuous with respect to neutron energy. Figure 4 of Ref. [12] shows that the magnitude of the neutron flux simulated by GEANT4 increases with the energy of the incident proton beam. However, it is remarkable that the neutron spectra are rather flat at neutron energies above 5 MeV and then drop sharply at the neutron energies close to the incident proton energies.

Let us denote by $\Phi_{Ep}(E_n)$ the neutron spectrum generated by the incident proton energy E_p. If we subtract $\Phi_{35}(E_n)$ from $\Phi_{40}(E_n)$, the difference $\Delta\Phi_1 = \Phi_{40}(E_n) - \Phi_{35}(E_n)$ can be obtained. Likewise, the difference $\Delta\Phi_2 = \Phi(E_{35}) - \Phi(E_{30})$ can be obtained. These two distributions are plotted in Fig. 1, and the two deduced peaks can be fitted by Gaussian functions.

When the peak of the difference $\Delta\Phi_1(E_n) = \Phi_{40}(E_n) - \Phi_{35}(E_n)$ is fitted by a Gaussian function, the central value of the peak is 34.8 MeV with the width of 3.6 MeV. Similarly, $\Delta\Phi_2(E_n) = \Phi_{35}(E_n) - \Phi_{30}(E_n)$ is fitted with the peak energy of 29.8 MeV and the width of 3.6 MeV. These central values agree well with the flux-weighted average energies defined by

$$\langle E_n \rangle = \frac{\int_{E_c}^{E_{\max}} E_n \Delta\Phi(E_n)\, dE_n}{\int_{E_c}^{E_{\max}} \Delta\Phi(E_n)\, dE_n}. \quad (1)$$

[a] e-mail: swhong@skku.ac.kr

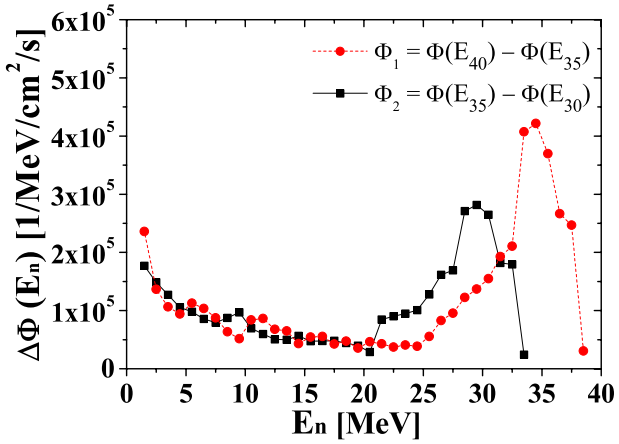

Figure 1. The difference spectra of the simulated neutron spectra. The red dotted and black solid curves are for the $\Delta\Phi_1(E_n) = \Phi_{40}(E_n) - \Phi_{35}(E_n)$ and $\Delta\Phi_2(E_n) = \Phi_{35}(E_n) - \Phi_{30}(E_n)$, respectively.

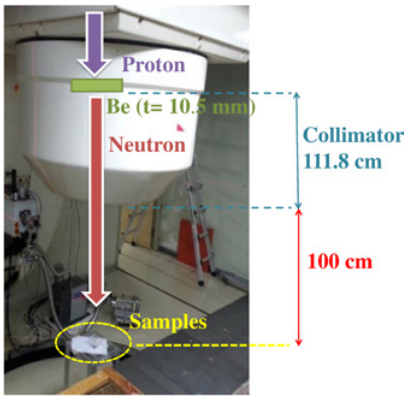

Figure 2. The geometry of the Be target, the neutron collimators, and the sample target.

In Eq. (1), the cut-value E_c is chosen as 31 MeV and the maximum energy $E_{\max}$ is chosen as 39 MeV for the $\Delta\Phi_1(E_n)$, and E_c and $E_{\max}$ for $\Delta\Phi_2(E_n)$ are 26 and 34 MeV, respectively.

3. Experiments

The experiment was conducted by using the MC-50 cyclotron at KIRAMS. This cyclotron provides proton beams in the range from 20 to 50 MeV at a maximum beam current close to 50 μA. In the present work we used three proton beam energies of 30, 35, and 40 MeV and the beam current of 20 μA.

The samples used for the experiment were of two types; one is yttrium oxide powder (99.99% pure) with an average mass of 3.03 g (for the three Y samples used) and another is a noibium powder (99.95% pure) with an average mass of 3.02 g (for the three Nb samples used). These samples were placed downstream along the neutron beam at a distance of 100 cm from the bottom of the collimator as shown in Fig. 2. All the six samples are placed inside a circle of 6 cm radius, which corresponds to $\theta = 1.6^\circ$, where θ is the angle of the neutron momentum with respect to the incident proton beam direction. The irradiation time was 5400 s.

After irradiation, the gamma-ray activities from the produced isotopes were measured by a shielded ORTEC HPGe detector.

4. Data analysis

Experimentally measured activities of ^{88}Y or ^{87}Y are proportional to the integration of cross sections $\sigma(E_n)$ for ^{89}Y (n, 2n) or ^{89}Y (n, 3n) reactions multiplied by a neutron flux $\Phi(E_n)$,

$$A = N \int_{E_{th}}^{E_{\max}} \sigma(E_n)\,\Phi(E_n)\,dE_n, \tag{2}$$

where E_{th} is the threshold energy of each reaction, and N is a constant. By using a subtraction method [13], we can extract the cross sections at the central value of the neutron Gaussian peak. The cross section at the neutron energy of 34.8 MeV can be extracted by the following

$$\overline{\sigma} = \frac{\left(\frac{A_{40}}{N_{40}} - C\frac{A_{35}}{N_{35}}\right) - \int_{E_{th}}^{E_c} \sigma(E_n)\cdot(\Phi_{40}(E_n) - C\Phi_{35}(E_n))dE_n}{\int_{E_c}^{E_{\max}} (\Phi_{40}(E_n) - C\Phi_{35}(E_n))dE_n}, \tag{3}$$

where C is a factor to be explained shortly. We take the cross sections from the TENDL-2015 data library [14] for $\sigma(E_n)$ in Eq. (3), because the TENDL-2015 seems to reproduce best the EXFOR data for these reactions.

We remark that $\Delta\Phi_i$ (i = 1, 2) in Fig. 1 has non-zero values in the low energy regions while it is desirable that $\Delta\Phi_i = 0$ at low energies. Thus, in the calculation of the integrals in Eq. (3), the non-zero values of $\Delta\Phi_i$ can introduce errors in the analysis. To minimize the effect due to the non-zero values of $\Delta\Phi_i$ in the low energy region from the threshold energy (E_{th}) to a cut-value (E_c), we introduce a neutron flux cancellation factor by defining C as a factor which will make the integral

$$\int_{E_{th}}^{E_c} (\Phi_{40}(E_n) - C\Phi_{35}(E_n))\,dE_n \tag{4}$$

zero. The values of C is about 1.27 for $\Delta\Phi_1$ and is about 1.34 for $\Delta\Phi_2$.

Here we remark that the integrated experimental activities of ^{56}Mn and ^{24}Na from ^{56}Fe (n,p)^{56}Mn and ^{27}Al (n, α)^{24}Na reactions, respectively, are about 10% larger than those estimated by using the neutron flux shown in Fig. 4. of Ref. [12]. This 10% difference in the experimental and calculated activities may be traced to the uncertainty in the neutron flux. To check this uncertainty independently, we used a Nb powder to monitor the neutron flux. When Nb powders are placed together with Y samples, ^{92m}Nb are excited due to ^{93}Nb (n, 2n) reaction. We compared the experimentally measured activity with the calculated activity of ^{92m}Nb from^{93}Nb (n, 2n). The daughter nuclide ^{92m}Nb has $T_{1/2}$ = 10.15 d, and emits gamma-rays of energies E_γ = 934.44 keV. By detecting this gamma-ray, we obtained the overall correction factor (Z), which is defined by $Z = A^{cal}/A^{exp}$ where A is given by Eq. (2). Z is 0.86 for 30 MeV proton beam, 0.81 for 35 MeV proton beam, and 0.88 for 40 MeV proton beam.

5. Results

The reactions observed in this work are listed in Table 1, and the extracted cross sections for ^{89}Y (n, 3n) ^{87m}Y,

Table 1. The reactions observed and their characteristics.

Nuclear reaction	$T_{1/2}$	E_{th} [MeV]	E_γ [keV]	I_γ [%]
^{89}Y(n,3n)^{87m}Y	13.37 h	21.06	380.79	78.0
^{89}Y(n,3n)^{87}Y	79.8 h	21.06	388.53	82.0
			484.80	89.7
^{89}Y(n,2n)^{88}Y	106.65 d	11.61	898.04	93.7

Table 2. The cross sections extracted for ^{89}Y(n,3n)^{87m}Y, ^{89}Y(n,3n)^{87}Y and ^{89}Y(n,2n)^{88}Y reactions.

E_n [MeV]	Cross section [mb]		
	^{89}Y(n,3n)^{87m}Y	^{89}Y(n,3n)^{87}Y	^{89}Y(n,2n)^{88}Y
29.8 ± 1.8	352 ± 58	143 ± 16	312 ± 332
34.8 ± 1.8	498 ± 80	205 ± 34	817 ± 362

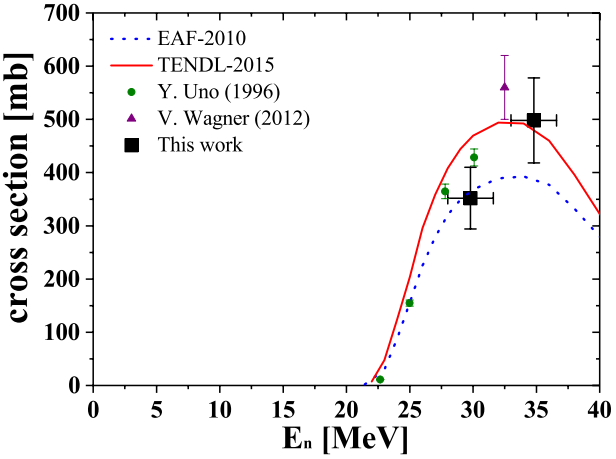

Figure 3. The cross sections extrated for ^{89}Y(n,3n)^{87m}Y are plotted by the squares at two neutron energies and are compared with the EXFOR data, TENDL and EAF cross sections.

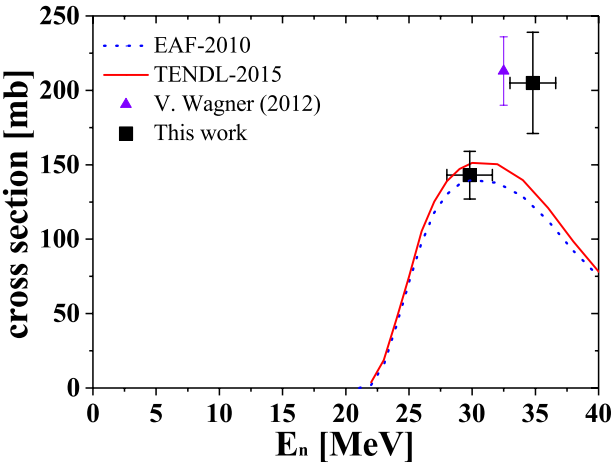

Figure 4. The cross sections extracted for ^{89}Y(n,3n)^{87}Y are plotted by the squares at two neutron energies and are compared with the EXFOR data, TENDL and EAF cross sections.

^{89}Y (n,3n) ^{87}Y and ^{89}Y (n,2n) ^{88}Y reactions are listed in Table 2. These results are compared with the EXFOR data [15], TENDL-2015, and EAF-2010 data libraries in Figs. 3–5. Our experimental data are found to be in fairly good agreement with other existing data, which indicates that measuring the (n, xn) cross sections by using neutron spectra with a continuous energy spectrum is possible.

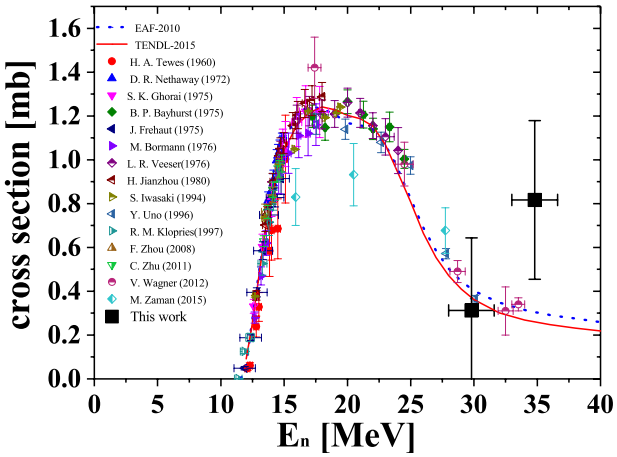

Figure 5. The cross sections extrated for ^{89}Y(n,2n)^{88}Y are plotted by the squares at two neutron energies and are compared with the EXFOR data, TENDL and EAF cross sections.

6. Summary

A proton cyclotron MC-50 in KIRAMS is used to carry out neutron activation experiments with Y_2O_3 targets irradiated with neutron beams of a continuous spectrum produced by proton beams on a thick beryllium target. By using a subtraction method, the cross section of ^{89}Y(n,2n) and ^{89}Y(n,3n) reactions at the neutron energies of 29.8 ± 1.8 MeV and 34.8 ± 1.8 MeV are extracted and are found to be close to the existing cross sections from the EXFOR data and the evaluated nuclear data libraries such as TENDL-2015 or EAF-2010. We show continuous energy neutron spectra can be used to extract the (n, xn) cross sections.

This work was supported in part by the Nuclear Energy Research Infrastructure Program through the Korea National Research Foundation (2013R1A1A2063824, 2015M2B2A4032926, 2015M2B2A9032869 and 2015M2A2A4A01045320).

References

[1] Y. Kadi, J.P. Revol, *Design of an accelerator-driven system for the destruction of nuclear waste*, Lectures given at the Workshop on Hybrid Nuclear Systems for Energy Production, Utilisation of Actinides & Transmutation of Long-Lived Radioactive Waste. Trieste, 3–7 September 2001
[2] D.R. Nethaway, Nucl. Phys. A **190**, 635 (1972)
[3] L.R. Veeser, E.D. Arthur, P.G. Young, Phys. Rev. C **16**, 1792 (1977)
[4] J. Vrzalová, O. Svoboda, A. Krása, A. Kugler, M. Majerle, M. Suchopár, V. Wagner, Nucl. Instrum. Methods Phys. Res. Sect. A **726**, 84 (2013)
[5] V. Wagner, M. Suchopár, J. Vrzalová, P. Chudoba, T. Herman, O. Svoboda, B. Geier, A. Krása, M. Majerle, A. Kugler, J. Phys. Conf. Ser. **533**, 012052 (2014)
[6] C. Guerrero, et al., Eur. Phys. J. A **49**, 27 (2013)
[7] W. Mondelaers, P. Schillebeeckx, *GELINA, a neutron time-of-flight facility for high-resolution neutron data measurements*, Notiziario neutroni e luce di sincrotrone, **11**, 19 (2006)
[8] H. Harano, N. Ralf, Metrologia **48**, S292 (2011)

[9] M. Ibaraki, M. Baba, T. Miura, T. Aqki, T. Hiroishi, H. Nakashima, S.I. Meigo, S. Tanaka, J. Nucl. Sci. Technol. **39** 405 (2002)
[10] S. Agostinelli, et al., Nucl. Instrum. Methods Phys. Res. Sect. A **506**, 250 (2003)
[11] J.W. Shin, T.-S. Park, Nucl. Instrum. Methods Phys. Res. Sect. B **342** 194 (2015)
[12] J.W. Shin, S.-I. Bak, C.M. Ham, E.J. In, K.J. Min, Y. Zhou, T.-S. Park, S.-W. Hong, V.N. Bhoraskar, Nucl. Instrum. Methods Phys. Res. Sect. A **797**, 304 (2015)
[13] J.K. Park, S. Kwon, S.W. Lee, J.T. Kim, J.-S. Chai, J.W. Shin, S.W. Hong, J. Korean Phys. Soc. **58** 1511 (2011)
[14] `https://tendl.web.psi.ch/tendl_2015/neutron_html/neutron.html`
[15] `http://www-nds.iaea.org/exfor`